

High quality factor microcavity lasers realized by circular photonic crystal with isotropic photonic band gap effect

Po-Tsung Lee, Tsan-Wen Lu, Jyun-Hao Fan, and Feng-Mao Tsai

Citation: [Applied Physics Letters](#) **90**, 151125 (2007); doi: 10.1063/1.2724899

View online: <http://dx.doi.org/10.1063/1.2724899>

View Table of Contents: <http://scitation.aip.org/content/aip/journal/apl/90/15?ver=pdfcov>

Published by the [AIP Publishing](#)

Articles you may be interested in

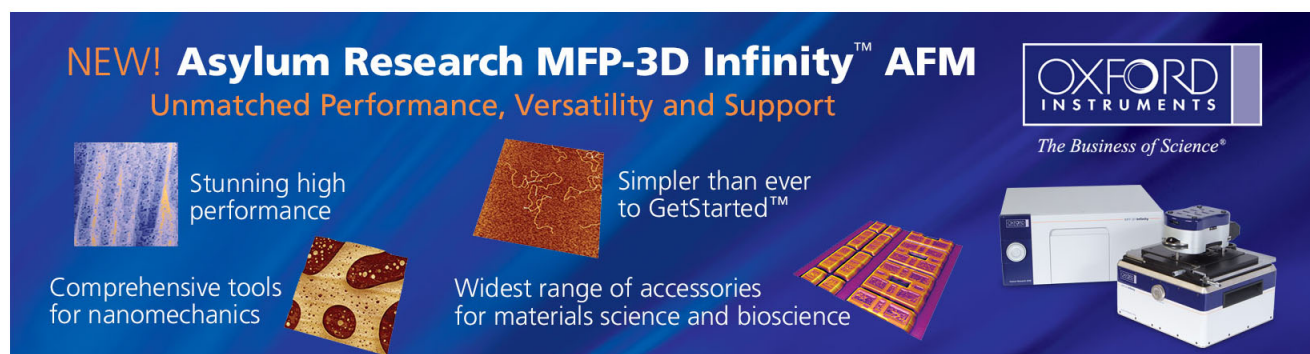
[Photonic crystal heteroslab-edge microcavity with high quality factor surface mode for index sensing](#)
Appl. Phys. Lett. **94**, 141110 (2009); 10.1063/1.3117225

[Investigation of whispering gallery mode dependence on cavity geometry of quasiperiodic photonic crystal microcavity lasers](#)
Appl. Phys. Lett. **89**, 231111 (2006); 10.1063/1.2402894

[High-quality-factor photonic crystal heterostructure laser](#)
Appl. Phys. Lett. **89**, 101104 (2006); 10.1063/1.2345912

[Quasiperiodic photonic crystal microcavity lasers](#)
Appl. Phys. Lett. **84**, 4875 (2004); 10.1063/1.1762705

[Experimental demonstration of a high quality factor photonic crystal microcavity](#)
Appl. Phys. Lett. **83**, 1915 (2003); 10.1063/1.1606866

The advertisement features a dark blue background with white and orange text. At the top left, it reads 'NEW! Asylum Research MFP-3D Infinity™ AFM' in large white letters, followed by 'Unmatched Performance, Versatility and Support' in orange. On the right, the Oxford Instruments logo is shown with the tagline 'The Business of Science®'. Below the text are four images: a textured surface, a circular pattern, a grid of small squares, and the AFM instrument itself. Text descriptions are placed around these images: 'Stunning high performance' next to the textured surface, 'Simpler than ever to GetStarted™' next to the circular pattern, 'Comprehensive tools for nanomechanics' next to the grid, and 'Widest range of accessories for materials science and bioscience' next to the AFM instrument.

High quality factor microcavity lasers realized by circular photonic crystal with isotropic photonic band gap effect

Po-Tsung Lee, Tsan-Wen Lu,^{a)} Jyun-Hao Fan, and Feng-Mao Tsai

Department of Photonics and Institute of Electro-Optical Engineering, National Chiao Tung University, Rm. 415, CPT Building, 1001 Ta-Hsueh Road, Hsinchu, 300 Taiwan, Republic of China

(Received 12 February 2007; accepted 15 March 2007; published online 13 April 2007)

The photonic band gap (PBG) effect and its isotropy of sunflower-type circular photonic crystal (CPC) are obtained and investigated from the transmission spectra performed by finite-difference time-domain (FDTD) method. The PBG directional width variation is found to be only 6.7%. A well-confined whispering gallery mode (WGM) with azimuthal number of 6 is obtained by FDTD simulation from the CPC microcavity formed by seven missing air holes (C2). Ascribed to the deep and isotropic PBG confinement, the WGM lasing with very-low threshold (~ 0.13 mW) and very-high-quality (Q) factor ($>10\,000$) is obtained from well-fabricated CPC C2 microcavity lasers. © 2007 American Institute of Physics. [DOI: 10.1063/1.2724899]

In advanced optical communication systems, circular resonator plays a key role in numerous applications including filters, add/drop channel devices, optical buffer components, and so on. In most circular resonators with large dimension, they usually exhibit excellent characteristics of low loss, good confinement, high quality factor, etc. Unfortunately, when the size of resonator is reduced for condensed system requirement, the bend loss of total internal reflection arisen from decreased local radius of resonator increases dramatically. To solve this problem, a resonator design named annular circular resonator (ACR) is proposed by Scheue and Yariv.^{1,2} In ACR, the confinement is provided by Bragg reflection of the surrounded annular Bragg reflector formed by concentric periodic circular trenches instead of total internal reflection effect. However, there are two problems in ACR. First, the widely used membrane structure cannot be applied in ACR due to the annular Bragg reflector. Second, the current injection structure cannot be achieved due to its discontinuous structure. Very recently, one promising solution called circular photonic crystal (CPC) microcavity is proposed by several groups.³⁻⁶ In CPC microcavity, the circular trenches (annular Bragg reflector) are replaced by CPC lattices consisting of air holes fabricated on dielectric materials, as illustrated in Fig. 1(a), and the confinement is provided by the photonic band gap (PBG) effect of CPC lattice which is found very recently.^{7,8} In general, the CPC lattices are arranged to be concentric circles in different formations including square, triangular, and sunflower type.⁵ There are several advantages of using CPC microcavity. First, the isotropic PBG can be obtained from this kind of nonperiodic lattice structure due to its high symmetry in the wave vector (k) space. This implies that the CPC microcavity could provide more uniform confinement in different directions and lead to better lasing properties. Second, by proper design, the highly confined whispering gallery mode (WGM), which is a highly potential mode in photonic integrated circuits (PIC), can be sustained in the CPC microcavity. Third, due to the lattice geometry, the CPC microcavity fused with CPC waveguide^{7,9,10} also shows large flexibility in PIC design.

Although few theoretical results of modal characteristics of large microcavities ($>2\ \mu\text{m}$ in diameter) formed by CPCs have been reported,³⁻⁵ the characteristics of CPC microcavity with small cavity size ($<2\ \mu\text{m}$ in diameter) have not been studied yet. In this report, at first, we investigate the isotropy of the PBG of sunflower-type CPC by finite-difference time-domain (FDTD) simulations. Then we design a microcavity formed by seven missing air holes, called CPC C2 microcavity ($<2\ \mu\text{m}$ in diameter). Its modal characteristics performed by FDTD simulations indicate that the WGM can be sustained in this microcavity. From the well-fabricated devices, the WGM single-mode lasing action with ultralow threshold

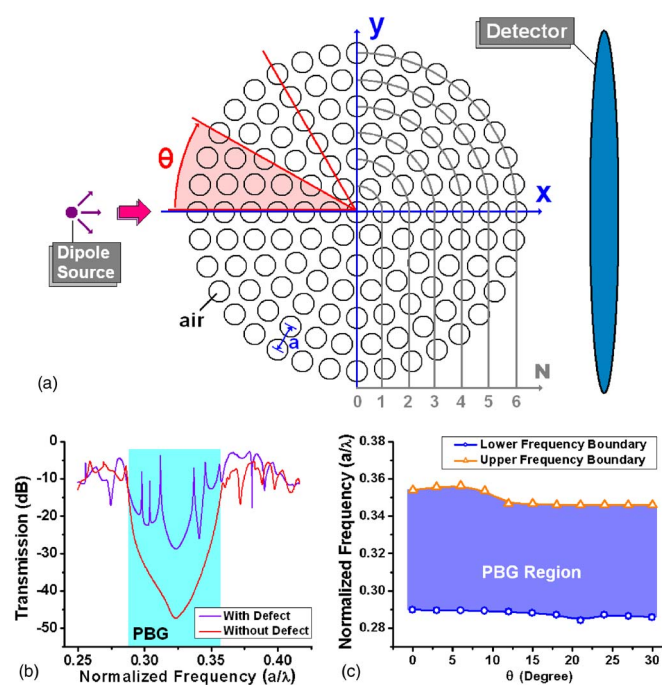


FIG. 1. (Color online) (a) Scheme of sunflower-type CPC lattice structure and the calculation setup of transmission spectrum. (b) Calculated transmission spectra of CPC lattice structure (red curve) and that with C2 microcavity (purple curve). The spectrum indicates the PBG region for normalized frequency from 0.29 to 0.354. (c) By rotating the whole CPC lattice, the variations of PBG width and upper and lower gap boundaries are calculated, which are 6.7%, 7.9%, and 4.5%, respectively, compared to PBG width at 0°.

^{a)}Electronic mail: ricky.eo94g@nctu.edu.tw

and estimated measured high quality (Q) factor is obtained.

The scheme of a sunflower-type CPC lattice is shown in Fig. 1(a), and the spatial lattice positions on the x - y plane are given by

$$x = aN \cos\left(\frac{2n\pi}{6N}\right), \quad y = aN \sin\left(\frac{2n\pi}{6N}\right), \quad n = 1 \sim 6N,$$

where a and N denote the lattice constant and number of the concentric lattice periods, which are also defined in Fig. 1(a). To investigate its PBG effect, we calculate its transmission spectrum using FDTD method with effective index approximation. A Gaussian dipole source with 0.366 central normalized frequency is put on one side of the CPC lattice formed by 127 air holes. Then, the transmitted electromagnetic wave is detected by a detector on the opposite side. The calculated transmission spectrum of CPC with 500 nm lattice constant (a) and 0.42 a air-hole radius (r) is shown as red curve in Fig. 1(b). In this figure, a significant PBG region lower than -15 dB transmission for normalized frequency from 0.29 to 0.354 is observed. To investigate the PBG isotropy, we rotate the CPC lattice by an angle θ with 3° increment, as shown in Fig. 1(a). In the simulation, we only deal with the case of $\theta = 0^\circ - 30^\circ$ due to the 12-fold-like rotational symmetry of CPC lattice. The normalized frequency of upper and lower gap boundaries as a function of θ is shown in Fig. 1(c). The variations of PBG width and upper and lower boundaries compared to the PBG width (defined at 0°) are only 6.7%, 7.9%, and 4.5%, respectively, which shows the isotropic PBG of CPC. (This result is quite similar with the CPC PBG isotropy using metallic rods reported by Horiuchi *et al.*⁸) We also numerically study the PBG directional variation of triangular photonic crystal (PC) for comparison by the same simulation setup. Its PBG width variation is found to be 10.1%, which is larger than that of CPC. Besides, the transmission depth (low transmission region) variation of PC PBG is about 15 dB, which is also much larger than 5 dB of CPC PBG. Thus, the above numerical results clearly indicate the isotropic PBG of CPC. In chasing for thresholdless micro- and nanoscale laser sources, the reduction of unnecessary spontaneous emission by the PBG effect becomes a key issue.¹¹ To suppress the spontaneous emission efficiently, the directional difference of PBG has to be relatively small compared to the width of PBG itself,⁸ i.e., the PBG must be isotropic. As a result, the CPC with isotropic PBG can be considered as a potential candidate of lattice structure to realize thresholdless laser sources.

The modal characteristics of CPC C2 microcavity are also performed by FDTD method with an effective index of 2.7, which is obtained with the dielectric slab thickness of 220 nm. In searching for defect modes in PC microcavity, FDTD method with effective index has been reported as a fast and reliable approach.¹² The normalized frequencies of calculated defect modes versus r/a ratio of CPC C2 microcavity are shown in Fig. 2. Lots of defect modes exist within the PBG region and their mode profiles are also shown in Fig. 2, including zero- ($K=4,5,6$), first- ($K=2,3$), and second-order ($K=0,1$) radial modes, where K denotes the rotational Bloch number. It is worthy to notice that one of them presents zero-order radial WGM profile with azimuthal number of 6 ($K=6$). The transmission spectrum of CPC C2 microcavity is also shown as purple curve in Fig. 1(b). For the researches in past decades, WGM is a very important

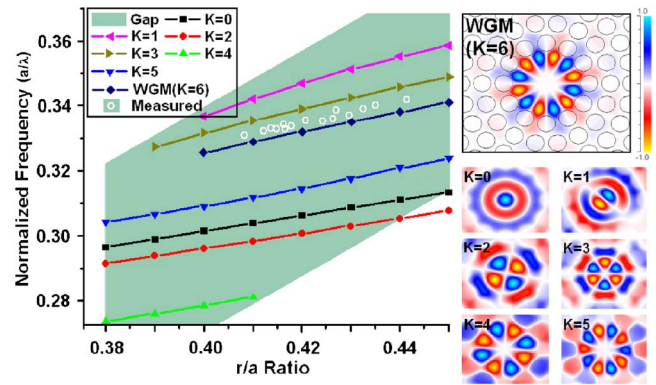


FIG. 2. (Color online) Defect modes in normalized frequency with different r/a ratios of CPC C2 microcavity are calculated by FDTD simulations. The defect mode profiles including zero- ($K=4,5,6$), first- ($K=2,3$), and second-order ($K=0,1$) radial modes are shown in the inset. The measured results denoted by open circles indicate that the lasing mode is WGM ($K=6$).

mode in the applications of quantum information process and coupled active devices with logical operation. But, in most photonic crystal microcavities, WGM is rarely well sustained in the cavity or takes the lead during mode competition. Thus, we will focus on this WGM in our following experiments and discussions.

In fabrication, the CPC C2 microcavity is fabricated on the epitaxial structure consisting of four 10 nm compressively strained InGaAsP multi-quantum-wells (MQWs) with 1550 nm peak wavelength and around 200 nm broad spectrum width from 1380 to 1580 nm under photoluminescence. The CPC patterns are defined by electron-beam lithography and transferred into MQWs by a series of inductively coupled plasma/reactive ion etching process. The membrane structure is formed by HCl selective wet etching. The details of the fabrication procedure can be found in our previous reports.^{13,14} The top-view and tilted-view scanning electron microscope (SEM) pictures of fabricated devices are shown in Fig. 3.

In characterization, the microcavity is optically pumped at room temperature by 845 nm laser pulse with 0.5% duty cycle. The measured lasing actions with different lattice parameters are denoted by open circles in Fig. 2, and they clearly indicate the lasing mode is WGM compared with the simulation results. The small difference between simulated and measured results is arisen from the index approximation used in FDTD simulations. The typical light-in-light-out (L-L) curve is shown in Fig. 4(a), and the threshold can be estimated as low as 0.13 mW from the curve. The spectra of near and above threshold at lasing wavelength of 1519.8 nm are shown in Figs. 4(b) and 4(c). The measured Q factor is larger than 10 000 estimated from measured linewidth

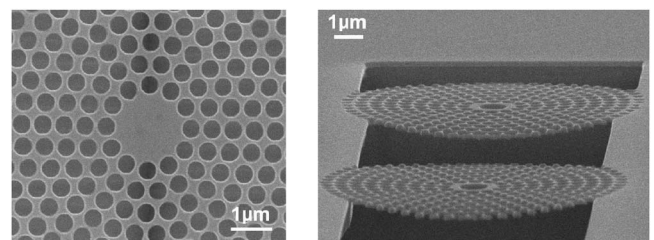


FIG. 3. Top-view (left) and tilted-view (right) SEM pictures of fabricated sunflower-type CPC C2 microcavities.

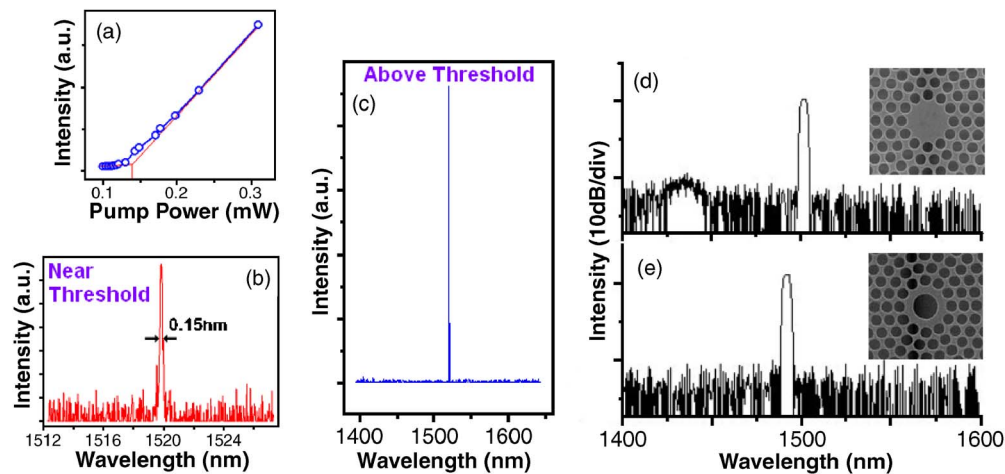


FIG. 4. (a) L - L curve and spectra of (b) near and (c) above threshold of WGM lasing action at 1519.8 nm for a typical CPC C2 microcavity. Its threshold and Q factor are estimated as 0.13 mW and over 10 000 from the L - L curve and the spectrum near threshold. Comparing the spectra of (d) before and (e) after adding a perturbation (central air hole) in CPC microcavity, the side mode is significantly reduced and the SMSR is increased up to 25 dB.

(Δ_{FWHM}) near the transparency pump level by $Q = \lambda / \Delta_{\text{FWHM}}$. This estimated Q factor value is limited to the resolution of our spectrum analyzer, and the details of this experimental estimated method can be found in report by Srinivasan *et al.*¹⁵ Comparing with the lasing characteristics of dodecagonal quasi-PC (DQPC) D2 microcavity we reported before,¹⁴ the estimated Q factor and the threshold of CPC C2 microcavity are both better than those of DQPC D2 microcavity. Actually, for these two microcavities, the cavity modal boundaries are almost the same. As a result, this indicates the more isotropic PBG confinement of CPCs than DQPCs. Besides, to further prove that the lasing mode is WGM, a direct approach is applying a perturbation in the microcavity, for example, fabricating a central air hole in the microcavity region.¹³ The typical lasing spectra in decibel scale are shown in Figs. 4(d) and 4(e). A significant side mode which is identified as dipole ($K=1$) mode can be observed in Fig. 4(d). After inserting the central air hole shown in the inset SEM picture, the side mode is greatly reduced without affecting the WGM lasing and the side-mode suppression ratio (SMSR) is increased up to 25 dB, as shown in Fig. 4(e). Besides, although the effective index of the microcavity is greatly reduced by this inserted central air hole, there is only small wavelength shifting under large cavity index variance, as shown in Figs. 4(d) and 4(e). This strongly implies the small influence caused by the central air hole on effective modal index of WGM, which provides direct evidence of WGM lasing.

Although above results in simulations and experiments show isotropic PBG of CPC and excellent performances of CPC C2 microcavity, small anisotropy still exists in the sunflower-type CPC due to its 12-fold-like symmetry in its Brillouin zone. In our undergoing work, to overcome this small anisotropy and realize real circular Brillouin zone, the CPC lattice structure needs to be modified. The approach is properly rotating the lattice structure period by period,^{4,8} and the further improved lasing properties of higher Q factor and lower threshold can be expected.

In summary, we have investigated the PBG isotropy of sunflower-type CPC lattice by FDTD simulated transmission spectra. The variations of PBG width and upper and lower

boundaries compared to PBG width at 0° are only 6.7%, 7.9%, and 4.5%, respectively, which indicate the isotropic PBG of CPC. The WGM ($K=6$) and other defect modes of CPC C2 microcavity are also calculated by FDTD method. From well-fabricated devices, we obtained the lasing action of WGM with high estimated Q factor of over 10 000 and ultralow threshold of 0.13 mW, which are ascribed to the isotropic CPC PBG effect. By adding extra perturbation (central air hole), we further confirm that the lasing mode is WGM and the SMSR is increased up to 25 dB due to the side-mode reduction.

This work is supported by Taiwan's National Science Council (NSC) under Contract Nos. NSC-95-2221-E-009-234 and NSC-95-2221-E-009-056 and Promoting Academic Excellence of Universities under Contract No. NSC-94-2752-E-009-007-PAE. The authors would like to thank the help from Tien-Chang Lu, Hao-Chung Kuo, and Center for Nano Science and Technology of National Chiao Tung University, Taiwan, R.O.C.

¹J. Scheuer and A. Yariv, *J. Opt. Soc. Am. B* **20**, 2285 (2003).

²J. Scheuer and A. Yariv, *IEEE J. Quantum Electron.* **39**, 1555 (2003).

³J. Scheuer and A. Yariv, *Phys. Rev. E* **70**, 036603 (2004).

⁴J. Chaloupka, J. Zarbakhsh, and K. Hingerl, *Phys. Rev. B* **72**, 085122 (2005).

⁵D. Chang, J. Scheuer, and A. Yariv, *Opt. Express* **13**, 9272 (2005).

⁶S. S. Xiao and M. Qiu, *Photonics Nanostruct. Fundam. Appl.* **3**, 134 (2005).

⁷J. Zarbakhsh, F. Haggmann, S. F. Mingaleev, K. Busch, and K. Hingerl, *Appl. Phys. Lett.* **84**, 4687 (2004).

⁸N. Horiuchi, Y. Segawa, T. Nozokido, K. Mizuno, and H. Miyazaki, *Opt. Lett.* **29**, 1084 (2004).

⁹N. Horiuchi, Y. Segawa, T. Nozokido, K. Mizuno, and H. Miyazaki, *Opt. Lett.* **30**, 973 (2005).

¹⁰S. S. Xiao and M. Qiu, *Phys. Lett. A* **340**, 474 (2005).

¹¹M. Fujita, S. Takahashi, Y. Tanaka, T. Asano, and S. Noda, *Science* **308**, 1296 (2005).

¹²Z. Qiang and W. Zhou, *IEEE Photonics Technol. Lett.* **18**, 1940 (2006).

¹³P. T. Lee, T. W. Lu, F. M. Tsai, T. C. Lu, and H. C. Kuo, *Appl. Phys. Lett.* **88**, 201104 (2006).

¹⁴P. T. Lee, T. W. Lu, F. M. Tsai, and T. C. Lu, *Appl. Phys. Lett.* **89**, 231111 (2006).

¹⁵K. Srinivasan, P. E. Barclay, O. Painter, J. Chen, A. Y. Cho, and C. Gmachl, *Appl. Phys. Lett.* **83**, 1915 (2003).